

High-Fidelity Structural Loads Analysis of the ONERA 7A Rotor

Hyeonsoo Yeo

US Army Aviation Development Directorate
Aviation & Missile Research, Development & Engineering Center
Research, Development, and Engineering Command
Ames Research Center, Moffett Field, CA, USA

Mark Potsdam

Biel Ortun

ONERA – The French Aerospace Lab
Meudon, France

Khiem Van Truong

ONERA – The French Aerospace Lab
Châtillon, France

ABSTRACT

The ONERA 7A rotor wind tunnel test data are investigated to assess the accuracy of analytical tools in the calculation of rotor airloads and structural loads. Comprehensive analysis codes, HOST and RCAS, and coupled computational fluid dynamics/comprehensive analysis codes, elsA/HOST and Helios/RCAS, are used to examine the ONERA 7A rotor blade dynamics, trim, airloads, and structural loads, and the calculated results are compared with the measured data for both high-speed and high-thrust conditions. The present elsA and Helios analyses include the test stand modeling. Comprehensive analyses show significant phase differences for the airloads and structural loads. The phase correlation is substantially improved by the coupled analyses for both high-speed and high-thrust conditions. In general, the coupled analyses also improve the half peak-to-peak correlation of structural loads compared to the comprehensive analyses. The majority of the predictions from the coupled analyses in half peak-to-peak blade structural loads are within 20% of the measured data. The present study shows unprecedented correlation of structural loads for the 7A rotor, consistently better than the previous structural loads correlation for the UH-60A rotor using Helios/RCAS analysis.

NOTATION

A	rotor disk area, πR^2
a	speed of sound, m/s
c	chord, m
C_L/σ	rotor lift coefficient, $L/\rho(\Omega R)^2 A \sigma$
C_X/σ	rotor propulsive force coefficient, $X/\rho(\Omega R)^2 A \sigma$
f_m	section pitching moment per unit length, Nm/m
f_n	section normal force per unit length, N/m
$M^2 c_m$	section pitching moment coefficient, $f_m/\frac{1}{2}\rho a^2 c^2$
$M^2 c_n$	section normal force coefficient, $f_n/\frac{1}{2}\rho a^2 c$
L	rotor lift, N
R	blade radius, m
V_∞	free-stream velocity, m/s
X	rotor propulsive force, N
α_s	shaft angle (positive for rearward tilt), deg
β_{1c}	longitudinal flapping, deg
β_{1s}	lateral flapping, deg

θ_o	collective, deg
θ_{1c}	lateral cyclic, deg
θ_{1s}	longitudinal cyclic, deg
μ	advance ratio, $V_\infty/\Omega R$
ρ	freestream density, kg/m ³
σ	rotor solidity, 0.084
Ω	rotor angular velocity, rad/s

INTRODUCTION

Rotor loads and vibration analysis is a challenging multi-disciplinary problem due to coupling of the complex structural deformations of rotor blades with the three dimensional and highly unsteady aerodynamic environment. Rotorcraft aeromechanics prediction capability using coupled computational fluid dynamics (CFD) / rotorcraft comprehensive analysis (CA) has advanced significantly in recent years. Comprehensive analyses based on multibody finite element modeling solve the complex structural dynamics of nonlinear elastic rotating blades. The CFD methods, which use a high fidelity, Navier-Stokes methodology with first principles-based wake capturing, perform three-dimensional and highly unsteady aerodynamics analysis. Coupling a CFD code to a

Presented at the 42nd European Rotorcraft Forum, Lille, France, September 5-9, 2016. This is a work of the U.S. Government and is not subject to copyright protection in the U.S. DISTRIBUTION STATEMENT A. Approved for public release; distribution is unlimited.

comprehensive code overcomes the limitations of the conventional lifting line aerodynamics used in rotorcraft comprehensive codes and produces the highest fidelity solution currently possible. This high-fidelity methodology has been extensively used to validate with flight and wind tunnel test data for the UH-60A rotor (Refs. 1–5), 40% Mach-scaled Bo105 main rotor for HART-II (Refs. 6, 7), and 7A/7AD rotors (Refs. 8–11). Despite the revolutionary breakthroughs in CFD/CA coupling methodology, there are still many challenges remaining in obtaining accurate rotor loads predictions over a wide range of rotor systems and operating conditions.

The US Army Aviation Development Directorate and the French ONERA (Office National d’Etudes et de Recherches Aéropatiales) have conducted research to investigate the airloads and structural loads of the ONERA 7A rotor under the auspices of the United States/France Project Agreement on Rotorcraft Aeromechanics and Human Factors Integration Research. The objective of this effort is to accurately predict the 7A rotor blade loads for various operating conditions using high-fidelity analyses and ultimately demonstrate the suitability of these analysis tools for the design of future rotor blades.

Prediction of 7A rotor airloads for a high-speed condition ($\mu = 0.4$) has been performed by many researchers of ONERA and DLR (German Aerospace Center) using various combinations of CFD/CA tools (Refs. 8–11). These coupled analyses, however, showed less than satisfactory blade section normal force and pitching moment correlation with the test data. Analysis results of 7A rotor structural loads, let alone measured structural loads, have not been published until recently. Surrey et al. (Ref. 12) investigated 7A rotor blade dynamic characteristics using both 1-D and 3-D structural dynamics analyses and examined airloads and structural loads at the same high-speed condition using two CFD/CA analyses. Ortun et al. (Ref. 13), as a part of the US Army/French ONERA cooperative research project, examined 7A rotor airloads and structural loads at not only the high-speed but also high-thrust conditions using two CFD/CA analyses and showed good agreement with the test data.

Reference 13 by the present authors made significant progress on the 7A rotor loads prediction. It investigated the effects of the pressure integration method on the airloads computation. The number of points used to integrate the measured pressure data (i.e. the number of pressure transducers) is much smaller than the grid points used for the CFD calculations. By integrating the CFD-calculated pressures at the same pressure transducer locations used in the measurements, calculated blade section airloads, especially pitching moments, agreed very well with the measured data. The paper also showed the effects of including the test stand model in the CFD analyses. The test stand generated upflow through the front of the rotor disk and downflow over the back of the rotor disk. The coupled CFD/CA analyses with the test stand improved trim, pressures, airloads, and structural loads correlation, showing by far the best correlation up to now.

Reference 13 focused on the effects of the test stand on pressures and airloads with CFD/CA analyses and showed

only limited airloads results with comprehensive standalone analyses. In order to complement the work of Ref. 13, the present paper investigates the ONERA 7A rotor blade dynamics, trim, airloads, and structural loads at both high-speed and high-thrust conditions using two comprehensive analyses and two coupled CFD/CA analyses. Detailed structural loads correlation results are shown, and the accuracy of the analyses are quantified by presenting the deviation of the calculated half peak-to-peak values of blade structural loads from the measured values.

DESCRIPTION OF THE TEST

The 7A rotor is a four-bladed fully articulated rotor, with a radius of 2.1 m and solidity, σ , of 0.084. The blade is of rectangular planform and uses two airfoils, the OA213 and OA209. The blade has -3.95 deg/m twist rate and the twist distribution is non-linear near the tip. The 7A rotor was tested in the ONERA S1MA transonic wind tunnel in 1991 (Fig. 1). The ONERA S1MA is a closed circuit atmospheric wind tunnel with a maximum speed near Mach 1, and has three exchangeable test sections with a diameter of 8 m. This wind tunnel test generated an extensive database covering several different speed and thrust conditions. The database provides rotor performance, blade section pressures and airloads, structural loads, and blade motions, allowing for the validation of both aerodynamic and structural models of analytical tools.

Figure 2 shows the blade planform along with the location of the airfoils used and the pressure and structural loads measurements. Absolute pressures were measured at five radial locations (50%, 70%, 82.5%, 91.5%, and 97.5%R). Blade structural loads were obtained from strain gages located at six radial locations (30%, 40%, 55%, 65%, 75%, and 85%R). Flap bending moments are available at all six radial locations. However, chord bending moments are available at three radial locations (30%, 40%, and 85%R) and torsion moments are available at five radial locations (30%, 40%, 55%, 65%, and 75%R) for the test conditions investigated in this paper. Blade pressure data were collected at a rate of 128 samples/rev (about 2.8° resolution) and blade strain gauge data were collected at a rate of 72 samples/rev (5° resolution). Both data sets were ensemble averaged over 30 rotor revolutions.

Data from two different wind tunnel test conditions are used in this study: high-speed (pt312) and high-thrust (pt293) conditions. The test conditions are listed in Table 1. The high-speed condition ($\mu = 0.4$, $C_L/\sigma = 0.063$) is characterized by transonic flow on the advancing blade side which causes high-vibratory hub loads. The high-thrust condition ($\mu = 0.3$, $C_L/\sigma = 0.100$) is characterized by dynamic stall on the retreating blade side. It should be noted that the propulsive force non-dimensionalized with the free-stream dynamic pressure ($\frac{1}{2}\rho V_\infty^2 A \sigma$) is a constant 0.10, corresponding to a constant drag coefficient.

The rotor was trimmed to satisfy the Modane flapping law ($\beta_{1s} = 0$, $\beta_{1c} = -\theta_{1s}$) in addition to the specified rotor lift and propulsive force using the rotor collective and cyclic controls and shaft angle.

DESCRIPTION OF ANALYTICAL METHODS

The analytical results were obtained using both standalone comprehensive analyses and coupled CFD/CA analyses. ONERA used elsA (Ref. 14) for CFD and HOST (Ref. 15) for CA, and US Army used Helios (Ref. 16) for CFD and RCAS (Ref. 17) for CA. Descriptions of each analysis and how they are coupled to produce a higher fidelity solution are provided in this section.

elsA

The elsA CFD code (Ref. 14), developed at ONERA, solves the unsteady Reynolds-Averaged Navier-Stokes (URANS) equations for both background Cartesian grids and blade curvilinear grids. Cartesian grid generation and overset grid assembly is done automatically by the pre- and post-processing tool Cassiopee (Ref. 18). The spatial discretization of the equations is performed with Jameson's cell-centered second order scheme, using 2nd and 4th order coefficients of artificial viscosity. The unsteady algorithm corresponds to a backward Euler scheme, with an implicit Gear scheme for the 2nd-order time integration. The time step is equivalent to 0.3 deg of blade rotation. Turbulence is taken into account by the Kok $k-\omega$ model, with SST corrections (Ref. 19) and Zheng limiter (Ref. 20). The flow is modeled as fully turbulent. The near-body grids of the blades are rotated and deformed following the blade motion and trim provided, through the loose coupling, by the rotorcraft comprehensive analysis HOST.

HOST

HOST (Helicopter Overall Simulation Tool) (Ref. 15) is a rotorcraft comprehensive analysis developed by Airbus Helicopters. HOST modeling of blade dynamics is multibody-like. The blade is represented as an assembly of rigid segments connected by virtual joints. Euler-beam modeling provides 3 degrees of freedom, namely the chordwise bending, the flapwise bending and the torsion. A modal reduction approach is used to reduce the number of degrees of freedom from a large system of equations. The aerodynamics of HOST is based on a lifting line approach based on airfoil look-up tables combined with a wake model. In this effort, among the several wake models available, a prescribed wake helical geometry was used. For the coupling with elsA, HOST airloads are corrected, via the delta method (Ref. 1), by the CFD airloads. The 7A rotor blade is modeled in HOST using 25 spanwise elements. Section lift, drag, and moment values for the OA213 and OA209 airfoils were obtained from airfoil look-up tables. A 6.0 deg azimuthal step size was used for the structural dynamic and trim calculations in HOST.

Helios

Helios (HELicopter Overset Simulations), developed by the US Army and the Department of Defense Computational Research and Engineering Acquisition Tools and Environments

Air Vehicles (CREATETM-AV) program (Refs. 16, 21), is a multidisciplinary computational platform for high fidelity rotorcraft analysis. Helios uses a multi-mesh paradigm with structured meshes in the near-body to capture the wall-bounded viscous effects and Cartesian grids in the off-body to resolve the wake through a combination of higher-order algorithms and adaptive mesh refinement (AMR). An overset procedure facilitates data exchange and also enables relative motion between meshes using the parallel domain connectivity solver PUNDIT (Parallel UNsteady Domain Information Transfer). In this effort Helios solves the near-body grids around the rotor blades with the CFD solver OVERFLOW (Ref. 22), using a 5th-order central difference scheme in space and a 2nd-order backward differentiation formula (BDF2) scheme in time. The Cartesian off-body grids are solved with SAMCart using a 5th-order central difference scheme in space and either a 3rd-order explicit 3-stage Runge-Kutta scheme or 2nd-order implicit lower-upper symmetric-Gauss-Seidel method (LU-SGS) BDF2 in time. The fully turbulent flow is modeled using the Spalart-Allmaras detached eddy simulation (DES) turbulence model in both the near- and off-body grids. The time step is equivalent to an azimuthal step size of 0.25 deg. AMR was not used.

RCAS

RCAS (Rotorcraft Comprehensive Analysis System) (Ref. 17), developed by the US Army, is a comprehensive multidisciplinary, computer software system for predicting rotorcraft aerodynamics, performance, stability and control, aeroelastic stability, loads, and vibration. The 7A rotor blade is modeled in RCAS using 16 nonlinear beam elements and 22 aerodynamic segments. Look-up tables of 7A blade airfoils were provided by ONERA so that the same airfoil tables are used for both HOST and RCAS analyses. The rotor hub was modeled as fully articulated with pitch bearing and flap and lag hinges. The elastomeric lag damper of the 7A rotor was modeled with equivalent hinge stiffness and damping values at the lag hinge. The present analytical model does not include test stand dynamics nor drive train dynamics. A 5.0 deg (72 steps per rotor revolution) azimuthal step size was used for the structural dynamic calculations in RCAS.

The RCAS standalone analysis was conducted using nonuniform inflow with prescribed wake geometry and unsteady aerodynamics based on classical quasi-steady Theodorsen theory (Ref. 23). Dynamic stall is very important for rotor loads at high-thrust conditions. Various semi-empirical dynamic stall models have been developed and integrated into comprehensive analyses. However, a dynamic stall model was not used for the current HOST and RCAS analyses because a consistent comparison between the two analyses was not possible due to convergence issues with a dynamic stall model.

CFD/CA coupled analysis

The CFD/CA coupling procedure used the standard loose or “delta” coupling approach. At each coupling iteration the aerodynamic loads calculated by CFD are passed to CA. After trimming with the CFD airloads, CA computes the blade deflections relative to the blade frame of reference and passes them back to CFD. This sequence is repeated until the airloads, deflections, and control angles converge. The trim parameters used in the predictions were the same as those from the test, a four degree-of-freedom trim. The trim targets are the specified rotor lift, rotor propulsive force and the Modane flapping law ($\beta_{1s} = 0, \beta_{1c} = -\theta_{1s}$).

For consistency, the grids of the CFD problems are very similar between elsA and Helios. Both CFD codes use overlapping grids consisting of structured curvilinear near-body grids rotating in a Cartesian background grid of 10% chord spacing (Fig. 3). The computational grids model the 7A blade geometry and test stand, but do not include a hub or the wind tunnel walls. The size of the elsA grid is approximately 27M points. The Helios mesh is 120M points, including block splitting and fringe points. Because AMR is not used, a fixed refinement box is required to cover the entire rotor plane as well as the test stand and some distance downstream. The near-body grid of the 7A rotor blade has 233x201x65 (around chord, spanwise, normal) nodes in elsA and 303x179x65 nodes in OVERFLOW. In both cases the main blades are O topology.

In the HOST and elsA/HOST analyses, the blade is represented by the first seven eigenmodes and the blade periodic response was calculated with up to seven harmonics. For the RCAS and Helios/RCAS analyses, although a modal analysis method is available, full finite element representation of the blade is maintained throughout the dynamic analysis and no harmonic truncation is used. Neither comprehensive analysis included blade structural damping, test stand dynamics, or drive train dynamics.

RESULTS AND DISCUSSION

In this section, selected data from the wind tunnel test are compared with predictions from the two comprehensive analyses (HOST and RCAS) and the two coupled analyses (elsA/HOST and Helios/RCAS). These test data include blade frequencies, trim angles, blade section airloads, and blade structural loads for both high-speed and high-thrust conditions.

Rotor blade dynamics

First, 7A rotor structural dynamics models were developed using HOST and RCAS comprehensive analysis codes, non-rotating natural frequencies are calculated, and the analysis results are compared with experimental measurements, as shown in Fig. 4. Comparisons are made for up to eight modes, which include five flap modes, two lag modes, and one torsion mode. In the shake test, the blade was clamped near the root (r

$= 0.275$ m, outboard of the pitch bearing) and the non-rotating natural frequencies were measured for each blade. The results from the shake test of the four blades showed that the variation among their modal frequencies is very small, mostly less than 1.0%. The measured frequency values averaged over each of the four blades are used for the comparison in Fig. 4. In general, there is good agreement between the two analyses and the calculated frequencies show reasonably good agreement with the experiment, except for the first torsion and fifth flap modes. RCAS underpredicts the first torsion frequency by about 3.3% while HOST overpredicts it by only about 0.5%. HOST overpredicts the fifth flap frequency by about 4.1% while RCAS underpredicts it by only about 0.3%.

Figure 5 compares the blade in-vacuo natural frequencies calculated by HOST and RCAS as a function of the rotor speed. Unlike the clamped blade, this blade model includes both flap/lag hinges and pitch bearing. The frequencies shown here are for a nominal zero collective pitch. Measured frequencies at zero RPM are also presented for comparison. In general, the calculated non-rotating frequencies match well with the measured data except for the first torsion mode. Both analyses overpredict the first torsion frequency. The frequency predictions by the two comprehensive codes show excellent agreement with each other up to the fourth mode, however, the differences become larger for the higher frequency modes. The largest difference of about 2.5% was observed for the fourth flap mode at 100% RPM.

Trim angles for high-speed condition, $\mu = 0.4$, $C_L/\sigma = 0.063$ (pt312)

Figure 6 shows the calculated and measured blade pitch angles and shaft angle at the high-speed condition. HOST and elsA/HOST results are compared in Fig. 6(a), and RCAS and Helios/RCAS results are compared in Fig. 6(b). The coupled analysis results shown here include the test stand modeling. HOST shows reasonably good agreement of the measured blade pitch angles, except lateral cyclic angle which was underpredicted by about 1.7 deg. The coupled elsA/HOST analysis shows better agreement with the measured blade pitch angles, especially lateral cyclic, compared to the HOST standalone analysis. Both analyses, however, underpredict the magnitude of shaft angle by about 1.3 deg. As noted in Ref. 13, the coupled analyses underpredicted the lateral cyclic angle by about 2.1 deg without the test stand model, but the underprediction reduced to about 0.8 deg with the test stand. Although not shown here, a three degree-of-freedom trim was performed by specifying the measured shaft angle (propulsive force not matched with the measured value) and the calculated loads did not change because collective pitch was adjusted to compensate for the shaft angle change. Similar results are obtained from the RCAS standalone and coupled Helios/RCAS analyses. There is, in general, good agreement between the two comprehensive analyses and between the two coupled analyses.

Airloads for high-speed condition, $\mu = 0.4$, $C_L/\sigma = 0.063$ (pt312)

Blade section normal force and pitching moment for the high-speed condition are briefly examined in this section. More detailed pressure and airloads comparisons are available in Ref. 13. Figure 7 shows non-dimensional normal force at 82.5%R and 91.5%R and pitching moment at 91.5%R. As mentioned earlier, the current coupled analyses included the wind tunnel test stand and the integration of blade pressure to obtain sectional airloads from CFD is consistent with that used for the experimental data. For the comprehensive analyses based on lifting-line aerodynamics and airfoil tables, blade section airloads are calculated from airfoil section lift, drag and moment values based on the local section angle-of-attack and Mach number, and thus there is no integration of pressure involved. The test stand model cannot be included in the comprehensive analyses, either.

For the present 7A rotor case, the integration method had a negligible influence on the normal force. However, it significantly affected the pitching moment and the influence was larger on the advancing side and inboard on the blade. The pitching moment at 91.5%R was not affected much by the integration method and thus the same conclusion can be obtained regardless of the integration method used.

The rotor blade aerodynamic environment at high speed is characterized by compressibility, and negative lift and large aerodynamic pitching moment on the advancing blade. For the normal force comparison, the standalone comprehensive analyses show reasonably good correlation on magnitude, but the phase correlation is poor, which is a typical limitation of comprehensive analyses based on lifting-line aerodynamics (Ref. 1). The coupled analyses significantly improve the phase of the negative lift and waveform in the first quadrant. The current coupled analyses show significantly better correlation than previous studies (Refs. 8–11) for the 7A rotor using CFD/CA analyses. A large aerodynamic pitching moment on the advancing side is also better captured by the coupled analyses.

Structural loads for high-speed condition, $\mu = 0.4$, $C_L/\sigma = 0.063$ (pt312)

This section compares the calculated blade flap bending, chord bending and torsion moments with the wind tunnel test data for the high-speed condition. Figure 8 shows oscillatory flap bending moment at 30%R, 55%R, and 75%R. Steady values were removed from both test data and analyses. The measured data show that a 2/rev harmonic is dominant, which appears to be primarily affected by the second flap mode whose predicted frequency is about 2.4/rev. It is interesting to note that for other rotors examined in Ref. 24 the second flap frequencies ranged from about 2.7 to 2.9/rev (closer to 3/rev) and thus 3/rev harmonic flap responses were more dominant than 2/rev responses. The comprehensive analyses show significant phase differences, similar to the normal force correlation shown in Fig. 7. In general, the peak-to-peak amplitudes are

slightly better predicted by RCAS than HOST. The coupled analyses show better correlation with the data. Waveform and phase correlation is substantially improved at all azimuth angles by the coupled analyses. The high-frequency responses in the RCAS and Helios/RCAS analyses are from an 11.7/rev coupled flap/lag mode. There are several ways to eliminate or suppress this mode by using modal reduction, harmonic balance method, larger time step, adding structural damping, and so on. However, no attempt was made in this study to suppress the high-frequency responses. It is noted that this mode is not included in the HOST modal analysis.

Figure 9 shows oscillatory chord bending moments at 30%R, 40%R, and 85%R. The measured data show that a 3/rev harmonic is dominant and all the analyses capture this very well. The comprehensive analyses show significant phase differences and tend to overpredict the magnitude. Again, the coupled analyses significantly improve the phase correlation. The Helios/RCAS analysis also improves the amplitude correlation compared to the RCAS standalone analysis. Overprediction of peak amplitude around 315-degree azimuth was observed even with the coupled analyses. This overprediction was exacerbated by the inclusion of the test stand, especially for the elsA/HOST analysis (Ref. 13). It should be noted that the elsA/HOST analysis without the test stand model (e.g. isolated rotor only) showed much better amplitude correlation than that with the test stand model shown here, although the phase correlation was better with the test stand model (Ref. 13). Considering difficulties in accurate prediction of chord bending moment, especially for the UH-60A rotor (Refs. 5, 24), the present analyses show very good correlation with the test data.

Figure 10 shows oscillatory torsion moments at 30%R, 55%R, and 75%R. The measured torsion moments show stronger 5/rev content compared to the flap and chord bending moments. Both comprehensive analyses predict the peak-to-peak amplitudes reasonably well but show significant phase differences. Both comprehensive analyses also show bigger 6/rev than 5/rev responses. The coupled analyses capture the 5/rev content very well. The coupled analyses significantly improve phase, especially in the first and second quadrants. The peak-to-peak amplitudes are also well predicted except at 75%R where the elsA/HOST underpredicts.

In general, the structural loads correlation for the 7A rotor is consistently better than that for the UH-60A rotor presented in Ref. 3. This suggests that a lack of a complex hydraulic lag damper may simplify the analyses and that test stand and drivetrain dynamics, which were ignored, may not play a significant role in the 7A rotor analysis.

Trim angles for high-thrust condition, $\mu = 0.3$, $C_L/\sigma = 0.100$ (pt293)

This section investigates the high-thrust condition. Figure 11 shows the calculated and measured blade pitch angles and shaft angle. HOST and elsA/HOST results are compared in Fig. 11(a), and RCAS and Helios/RCAS results are compared

in Fig. 11(b). Comprehensive analyses underpredicted the trim angles, the largest difference being about 1.5-deg underprediction of lateral cyclic angle by RCAS. HOST underpredicts lateral cyclic angle by only about 0.7 deg. The coupled analyses show very good correlation of the trim angles, especially lateral cyclic correlation is excellent. Compared to the high-speed condition, the magnitude of shaft angle was more accurately predicted. The difference between the test and analyses for the shaft angle is less than 0.2 deg.

Airloads for high-thrust condition, $\mu = 0.3$, $C_L/\sigma = 0.100$ (pt293)

Blade section normal force and pitching moment for the high-thrust condition are briefly examined in this section. Figure 12 shows blade section normal force at 82.5%R and 91.5%R and pitching moment at 91.5%R. At this high thrust, aerodynamics is dominated by dynamic stall and large negative pitching moment on the retreating side. The comprehensive analyses predict very small pitching moment and thus were unable to capture the large azimuthal variations of pitching moment, especially a strong negative peak at around 290 deg. The RCAS analysis slightly better predicts the lift stall on the retreating side, although normal force correlation is not satisfactory on the advancing side. As mentioned before, a dynamic stall model was not used for the current comprehensive analyses. The coupled analyses significantly improve the normal force waveform in the first and second quadrants and capture lift and moment stall on the retreating side very well.

Structural loads for high-thrust condition, $\mu = 0.3$, $C_L/\sigma = 0.100$ (pt293)

This section compares the calculated blade flap bending, chord bending and torsion moments with the wind tunnel test data for the high-thrust condition. Figure 13 shows oscillatory flap bending moment at 30%R, 55%R, and 75%R. The measured data show that a 2/rev harmonic is dominant, same as the high-speed condition. The test data also show strong high frequency content which was not present for the high-speed condition. This 9/rev harmonic response is more prominent at the inboard section of the blade. At 75%R, the high frequency content is negligible. The comprehensive analyses show significant phase differences, consistent with the phase differences in the normal force shown in Fig. 12. In general, the peak-to-peak amplitudes are better predicted by RCAS than HOST, and this trend is the same as the high-speed condition. The coupled analyses show much better correlation with the test data. Waveform and phase correlation is substantially improved at all azimuth angles by the coupled analyses. The high-frequency responses are better captured in the RCAS and Helios/RCAS analyses. However, the predictions have a strong 12/rev harmonic which comes from the 11.7/rev coupled flap/lag mode, and the test data show a strong 9/rev harmonic which may come from the fifth flap mode whose predicted frequency is about 9.3/rev. It may be possible that the current RCAS analytical model has inaccurate natural frequency content for the high frequency modes, and these may

have affected the frequency content of the flap bending moments. The HOST and elsA/HOST analyses are limited to seven eigenmodes and seven harmonics, and therefore are not able to capture the high-frequency responses.

Figure 14 shows oscillatory chord bending moments at 30%R, 40%R, and 85%R. The measured data show that a 4/rev harmonic is dominant (note that a 3/rev harmonic was dominant for the high-speed condition) and both the comprehensive analyses and coupled analyses are able to capture this trend. The comprehensive analyses show significant phase differences and tend to underpredict the magnitude. Again, the coupled analyses significantly improve both magnitude and phase correlation. The elsA/HOST analysis shows very good correlation in both magnitude and phase, especially at 40%R. The Helios/RCAS analysis shows very good phase correlation, but underpredicts the peak-to-peak amplitude.

Figure 15 shows oscillatory torsion moments at 30%R, 55%R, and 75%R. The measured torsion moments show stronger high-frequency (both 5/rev and 6/rev) content compared to the flap and chord bending moments. The comprehensive analyses tend to underpredict the peak-to-peak amplitude and show phase differences. Both coupled analyses show very good correlation with the measured data, better capturing the high-frequency content and phase.

Quantitative structural loads correlation

In the design of rotor dynamic components, accuracies of fatigue life assessment of the components depend heavily on the accuracies of the estimated fatigue design loads (amplitude of oscillatory rotor loads). In order to characterize the accuracy of the present analytical tools for the design of a new rotor blade, the half peak-to-peak structural loads are examined quantitatively by comparing the analyses with the measured data. This is done in two ways. First, half peak-to-peak structural loads are plotted along the blade span. Then, plots of calculated half peak-to-peak loads vs. measured half peak-to-peak loads, termed “deviation”, are shown. These resulting plots graphically summarize the quantitative deviation of calculated results relative to measurements.

Figure 16 compares the HOST and elsA/HOST results with the measured data for flap bending, chord bending, and torsion moments at the high-speed condition. Both half peak-to-peak amplitude along the blade span and deviations from the measured data are shown. For the bottom row plots, the horizontal axes show the measured data and the vertical axes show the calculations. The 45-deg diagonal line represents a perfect agreement between analysis and test. The calculated half peak-to-peak loads lie above the 45-deg line if the analysis overpredicts, and below the line if the analysis underpredicts. Lines which represent a deviation of $\pm 20\%$ and $\pm 40\%$ from measurements are also shown to indicate correlation trends. A similar approach can be found for the half peak-to-peak structural loads correlation for the UH-60A, SA 330 (research Puma), SA 349/2, and H-34 rotors in forward flight by Ho and Yeo (Ref. 25).

In Fig. 16(a), the measured data show that half peak-to-peak flap bending moment slightly decreases from 30%R to 40%R, and increases to a peak at 65%R before it decreases further outboard. The HOST predictions also exhibit this behavior, but with up to 40% underprediction as shown in Fig. 16(d). The elsA/HOST predictions consistently improve the half peak-to-peak flap bending moment correlation along the blade span, and the predictions are mostly within about 20% underprediction of the measured data. As shown in Fig. 16(b), the measured half peak-to-peak chord bending moment appears to decrease continually from the blade root to tip. The HOST calculations capture this trend, but overpredict the measured data by more than 40% as shown in Fig 16(e). The elsA/HOST predictions show almost the same deviations as the HOST standalone analysis. As mentioned earlier, the elsA/HOST analysis without test stand showed better amplitude correlation than that with the test stand model (Ref. 13). Although not shown here, the deviation from the measured data is reduced to less than 20% without the test stand model. As shown in Fig. 16(c), the measured half peak-to-peak torsion moment decreases continually from the blade root to tip but the variation is small. The HOST predictions capture this trend very well and show very good correlation with the measured data. The elsA/HOST analysis shows almost perfect correlation up to 55%R, but underpredicts further outboard.

Figure 17 compares the RCAS and Helios/RCAS results with the measured data for flap bending, chord bending, and torsion moments at the high-speed condition. Figure 17(a) shows that the RCAS predictions agree well with the measured data at 30%R, 40%R and 75%R, but significantly underpredict at 65%R and overpredict at 85%R. The Helios/RCAS calculations slightly reduce the half peak-to-peak values and thus improve correlation at 85%R but worsen correlation at the other radial locations. With the exception of the RCAS prediction at 85%R and Helios/RCAS prediction at 65%R, both predictions are within 20% of the measured data as shown in Fig. 17(d). Figure 17(b) shows that the RCAS calculations overpredict the measured data by more than 40%, the same as the HOST calculations. The Helios/RCAS calculations reduce the half peak-to-peak values and significantly improve the correlation. The deviation from the measured data is less than 20% as shown in Fig. 17(e). Figure 17(c) shows that both RCAS and Helios/RCAS calculations exhibit similar accuracy in the prediction of the half peak-to-peak amplitude of torsion moments, although phase prediction was much better predicted by Helios/RCAS. Both calculations show very good correlation with the measured data. The deviation from the measured data are less than 15% as shown in Fig. 17(f)

Figure 18 compares the HOST and elsA/HOST results with the measured data for flap bending, chord bending, and torsion moments at the high-thrust condition. The HOST calculations underpredict the half peak-to-peak flap bending, chord bending and torsion moments along the blade span. The largest difference observed was about 54% underprediction of the half peak-to-peak flap bending moment at 65%R. The elsA/HOST predictions improve flap bending moment correlation near mid-span, chord bending moment correlation at all

radial locations and torsion moment correlation at 40%R and outboard locations. The elsA/HOST calculations of the half peak-to-peak chord bending moments are within 20% of the measured data.

Figure 19 compares the RCAS and Helios/RCAS results with the measured data for flap bending, chord bending, and torsion moments at the high-thrust condition. The RCAS calculations, the same as the HOST calculations, underpredict the half peak-to-peak flap and chord bending and torsion moments along the blade span. With the exception of torsion moment at 65%R, the RCAS calculations are within 40% of the measured data. The Helios/RCAS calculations show similar deviations as the RCAS calculations for the flap bending moment, but significantly improve the correlation of chord bending and torsion moments. The Helios/RCAS calculations of the half peak-to-peak chord bending and torsion moments are within 20% of the measured data.

SUMMARY AND CONCLUSIONS

The ONERA 7A rotor wind tunnel test data are investigated to assess the accuracy of analytical tools in the calculation of rotor airloads and structural loads for both high-speed and high-thrust conditions. Two comprehensive analysis codes, HOST and RCAS, and two coupled computational fluid dynamics/comprehensive analysis codes, elsA/HOST and Helios/RCAS, are used to examine the ONERA 7A rotor blade dynamics, trim, airloads, and structural loads, and the calculated results are compared with the measured data. The present elsA and Helios analyses include the test stand modeling. From this study, the following conclusions are obtained:

- 1) Non-rotating blade natural frequencies are calculated using HOST and RCAS, and the analysis results are compared with experimental measurements for the clamped boundary condition. There is good agreement between the two analyses, and the calculated frequencies show reasonably good agreement with the experiment, except for the first torsion and fifth flap modes.

- For the rotating frequency comparison, the predictions by the two comprehensive codes show excellent agreement with each other up to the fourth mode, however, the differences become larger for the higher frequency modes. The largest difference of about 2.5% was observed for the fourth flap mode at 100% RPM.

- 2) Trim angles (blade pitch angles and shaft angle) are reasonably well predicted by the comprehensive analyses, except the underprediction of lateral cyclic angle at both high-speed and high-thrust conditions due to a lack of test stand modeling. The coupled analyses show very good correlation of the trim angles, especially lateral cyclic correlation is excellent. Both comprehensive and coupled analyses underpredict the magnitude of shaft angle by about 1.3 deg at the high-speed condition, but predicted it accurately (less than 0.2 deg difference) at the high-thrust condition.

- 3) The coupled analyses significantly improve the phase of the negative lift at the high-speed condition and better capture

lift and moment stall on the retreating side at the high-thrust condition than the comprehensive analyses based on lifting-line aerodynamics without a dynamic stall model.

4) Comprehensive analyses show significant phase differences for the structural loads. The phase correlation is substantially improved by the coupled analyses for all the flap bending, chord bending and torsion moments at both high-speed and high-thrust conditions.

5) In general, the coupled analyses improve the half peak-to-peak correlation of structural loads compared to the comprehensive analyses. The Helios/RCAS calculations of the half peak-to-peak chord bending and torsion moments are within 20% of the measured data. The structural loads correlation for the 7A rotor is consistently better than that for the UH-60A rotor using the same Helios/RCAS analysis presented in Ref. 3.

REFERENCES

- ¹Potsdam, M., Yeo, H., and Johnson, W., "Rotor Airloads Prediction Using Loose Aerodynamic/Structural Coupling," *Journal of Aircraft*, Vol. 43, (3), May-June 2006.
- ²Datta, A., Nixon, M., and Chopra, I., "Review of Rotor Loads Prediction with the Emergence of Rotorcraft CFD," *Journal of the American Helicopter Society*, Vol. 52, (4), October 2007, pp. 287-317.
- ³Biedron, R. T., and Lee-Rausch, E. M., "An Examination of Unsteady Airloads on a UH-60A Rotor: Computation versus Measurement," American Helicopter Society 68th Annual Forum Proceedings, Forth Worth, TX, May 1-3, 2012.
- ⁴Sitaraman, J., Datta, A., Baeder, J., and Chopra, I., "Coupled CFD/CSD prediction of Rotor Aerodynamic and Structural Dynamic Loads for Three Critical Flight Conditions," 31st European Rotorcraft Forum, Florence, Italy, September 13-15, 2005.
- ⁵Yeo, H., and Potsdam, M., "Rotor Structural Loads Analysis Using Coupled Computational Fluid Dynamics/Computational Structural Dynamics," *Journal of Aircraft*, Vol. 53, (1), January-February 2016, pp. 87-105.
- ⁶Boyd Jr., D. D., "HART-II Acoustic Predictions using a Coupled CFD/CSD Method," American Helicopter Society 65th Annual Forum Proceedings, Grapevine, TX, May 27-29, 2009.
- ⁷Smith, M. J., Lim, J. W., van der Wall, B. G., Baeder, J. D., Biedron, R. T., Boyd Jr., D. D., Jayaraman, B., Jung, S. N., and Min, B. Y., "The HART II International Workshop: An Assessment of the State-of-the-Art in CFD/CSD Prediction," *CEAS Aeronautical Journal*, Vol. 4, No. 4, December 2013, pp. 345-372.
- ⁸Altmikus, A. R. M., Wagner, S., Beaumier, P., and Servera, G., "A Comparison: Weak versus Strong Modular Coupling for Trimmed Aeroelastic Rotor Simulations," American Helicopter Society 58th Annual Forum Proceedings, Montreal, Canada, June 11-13, 2002.
- ⁹Rodriguez, B., Benoit, C., and Gardarein P., "Unsteady Computations of the Flowfield around a Helicopter Rotor with Model Support," Paper AIAA 2005-466, 43rd AIAA Aerospace Sciences Meeting and Exhibit, Reno, NV, January 10-13, 2005.
- ¹⁰Beaumier, P., Costes, M., Rodriguez, B., Poinot, M., and Cantaloube, B., "Weak and Strong Coupling between the elsA CFD solver and the HOST Helicopter Comprehensive analysis," 31st European Rotorcraft Forum, Florence, Italy, September 13-15, 2005.
- ¹¹Pahlke, K., and van der Wall, B. G., "Chimera Simulations of Multibladed Rotors in High-Speed Forward Flight with Weak Fluid-Structure Coupling," *Aerospace Science and Technology*, Vol. 9, (5), July 2005.
- ¹²Surrey, S., Ortun, B., Truong, V. K., and Wienke, F., "Investigation of the Structural Blade Dynamics and Aeroelastic Behavior of the 7A Rotor," American Helicopter Society 72nd Annual Forum Proceedings, West Palm Beach, FL, May 17-19, 2016.
- ¹³Ortun, B., Potsdam, M., Yeo, H., and Truong, V. K., "Rotor Loads Prediction on the ONERA 7A Rotor using Loose Fluid/Structure Coupling," American Helicopter Society 72nd Annual Forum Proceedings, West Palm Beach, FL, May 17-19, 2016.
- ¹⁴Cambier, L., Heib, S., and Plot, S., "The ONERA elsA CFD software: input from research and feedback from industry," *Mechanics & Industry*, Vol. 14, 2013, pp. 159-174.
- ¹⁵Dequin, A. M., Benoit, B., Kampa, K., von Grünhagen, W., Basset, P. M., and Gimonet, B., "HOST, a General Helicopter Simulation Tool for Germany and France," American Helicopter Society 56th Annual Forum, Virginia Beach, VA, May 2-4, 2000.
- ¹⁶Wissink, A., Jayaraman, B., Datta, A., Sitaraman, J., Potsdam, M., Kamkar, S., Mavriplis, D., Yang, Z., Jain, R., Lim, J., and Strawn, R., "Capability Enhancements in Version 3 of the Helios High-Fidelity Rotorcraft Simulation Code," AIAA-2012-0713, 50th AIAA Aerospace Sciences Meeting, Nashville, TN, January 9-12, 2012.
- ¹⁷Saberi, H., Hasbun, M., Hong, J. Y., Yeo, H., and Ormiston, R. A., "Overview of RCAS Capabilities, Validations, and Rotorcraft Applications," American Helicopter Society 71st Annual Forum, Virginia Beach, VA, May 5-7, 2015.
- ¹⁸Benoit, C., Péron, S., and Landier, S., "Cassiopee: A CFD pre- and post-processing tool," *Aerospace Science and Technology*, Vol. 45, 2015, pp. 272-283.
- ¹⁹Menter, F. R., "Two-Equation Eddy-Viscosity Transport Turbulence Model for Engineering Applications," *AIAA Journal*, Vol. 32, 1994, pp. 1598-1605.

²⁰Zheng, X., Liao, C., Liu, C., Sung, C. H., and Huang, T. T., "Multigrid Computation of Incompressible Flows using Two-Equation Turbulence Models," *Journal of Fluid Engineering*, Vol. 119, 1997, pp. 893-905.

²¹Wissink, A., Sitaraman, J., Jayaraman, B., Roget, B., Lakshminarayan, V., Potsdam, M., Jain, R., Leffell, J., Forsythe, J. R., and Bauer, A., "Recent Advancements in the Helios Rotorcraft Simulation Code," AIAA-2016-0563, 54th AIAA Aerospace Sciences Meeting, January 4-8, 2016, San Diego, CA.

²²Nichols, R. H., and Buning, P. G., "OVERFLOW User's Manual, Version 2.2," NASA Langley Research Center, Hampton, VA, August 2010.

²³Theodorsen, T., "General Theory of Aerodynamic Instability and the Mechanism of Flutter," NACA Report 496, January 1949.

²⁴Yeo, H., and Johnson, W., "Prediction of Rotor Structural Loads with Comprehensive Analysis," *Journal of the American Helicopter Society*, Vol. 53, (2), April 2008, pp. 193-209.

²⁵Ho, J. C., and Yeo, H., "Assessment of Comprehensive Analysis Predictions of Helicopter Rotor Blade Loads in Forward Flight," American Helicopter Society 72nd Annual Forum Proceedings, West Palm Beach, FL, May 17-19, 2016.

Table 1. 7A rotor test conditions

Parameter	High-speed (pt312)	High-thrust (pt293)
Density, kg/m ³	1.002	1.018
Temperature, °C	23.9	27.9
Rotor speed, rpm	1012	1022
Airspeed, m/s	89.4	67.5
Advance ratio, μ	0.40	0.30
Rotor lift coefficient, C_L/σ	0.063	0.100
Rotor propulsive force coefficient, C_X/σ	0.0082	0.0046



Fig. 1. 7A rotor mounted in the ONERA Modane S1MA Wind Tunnel.

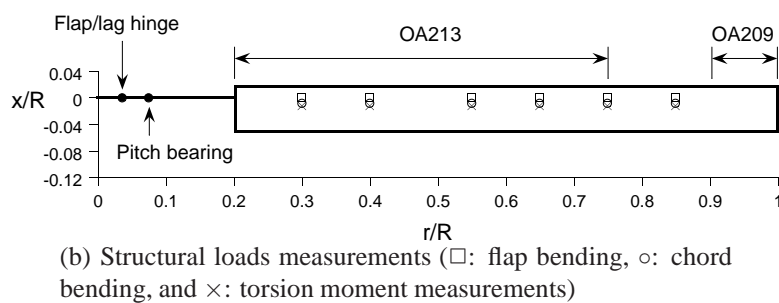
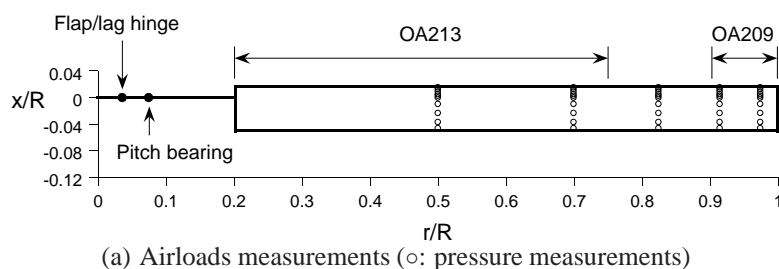
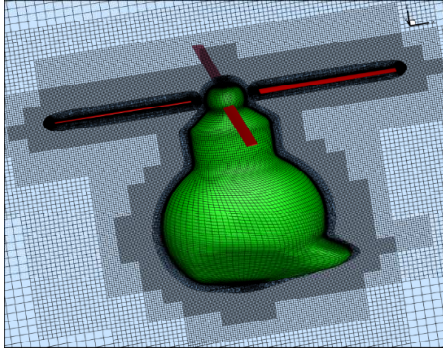
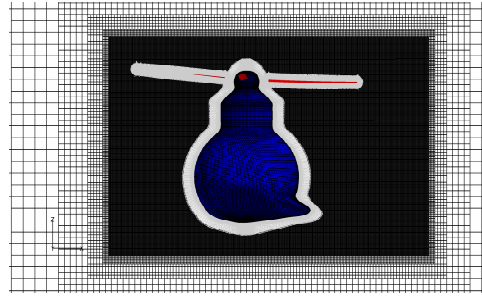


Fig. 2. Blade planform



(a) elsA



(b) Helios

Fig. 3. Overset grid systems.

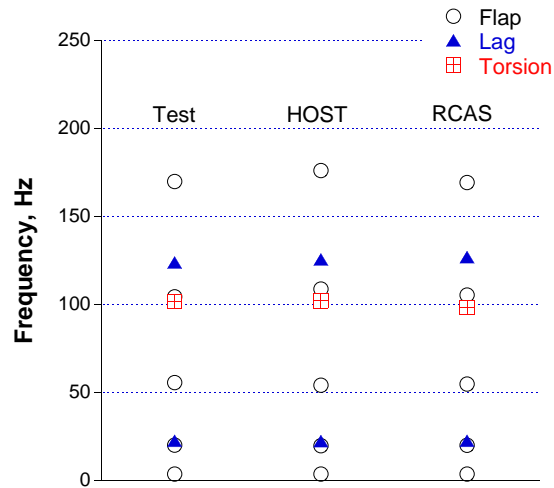


Fig. 4. Non-rotating natural frequency comparison of a clamped blade.

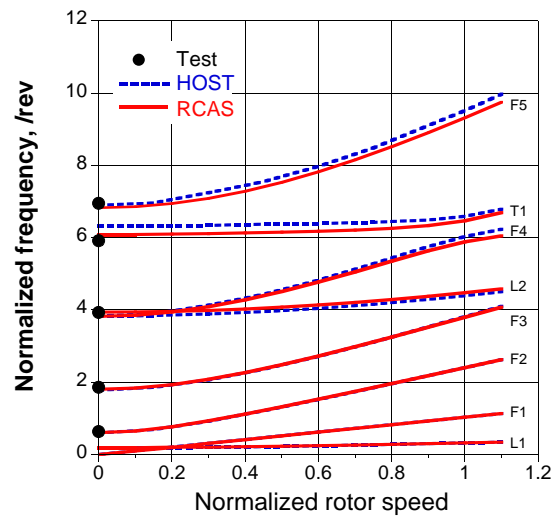


Fig. 5. Rotor blade natural frequency comparison.

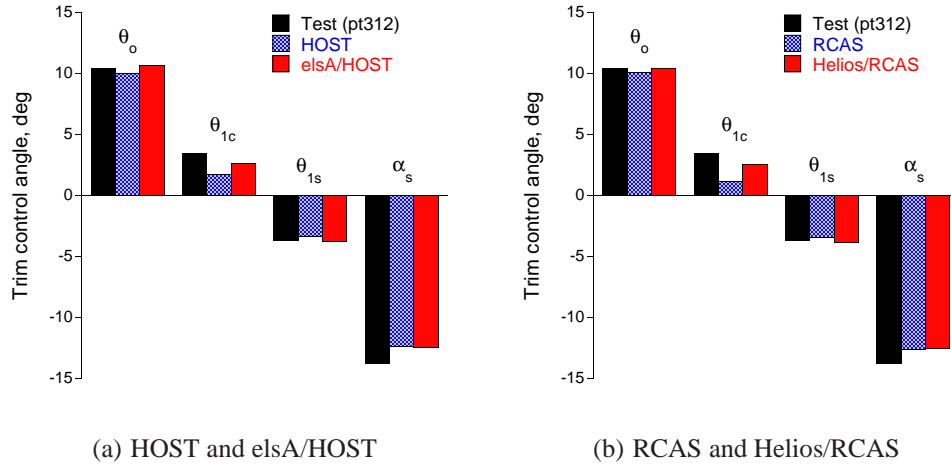


Fig. 6. Trim control angles at high-speed condition, $\mu = 0.4$, $C_L/\sigma = 0.063$.

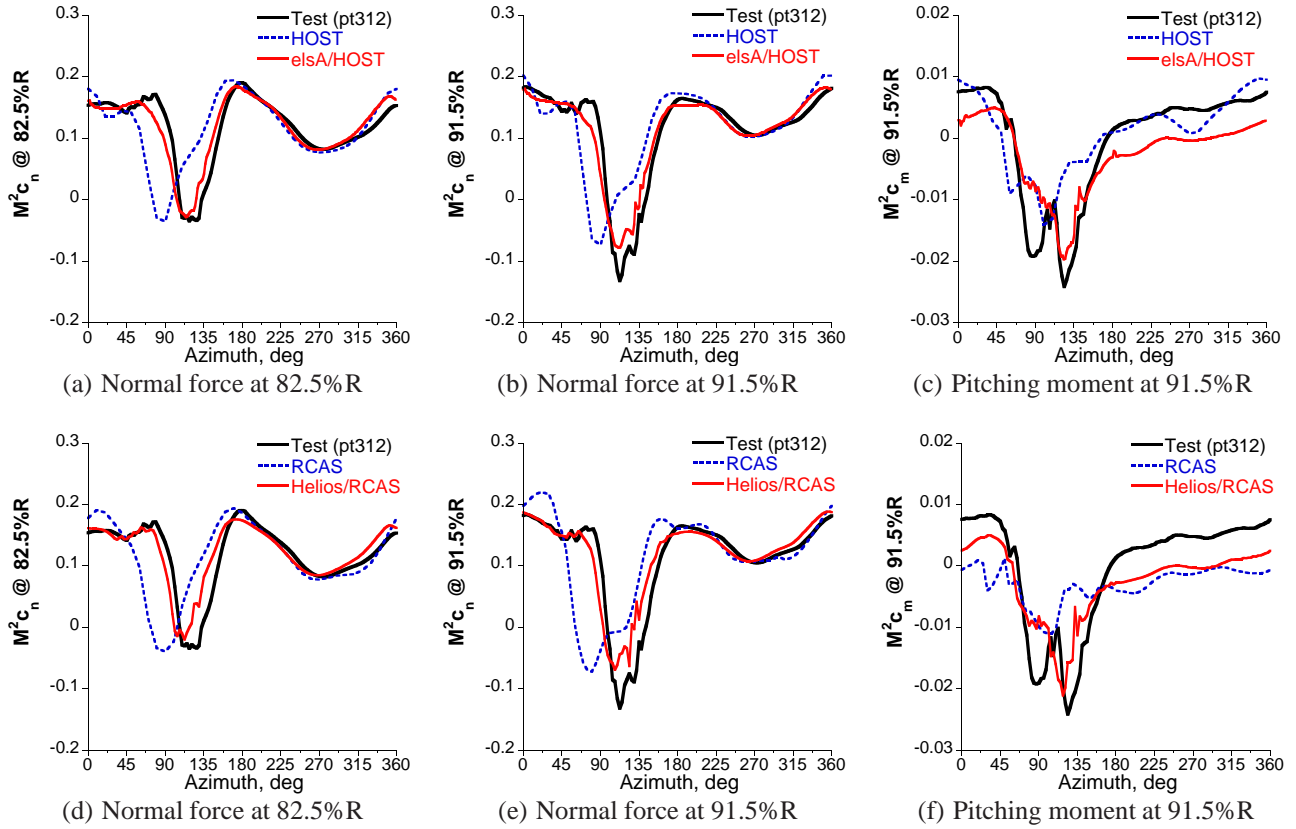


Fig. 7. Blade normal force and pitching moment at high-speed condition, $\mu = 0.4$, $C_L/\sigma = 0.063$.

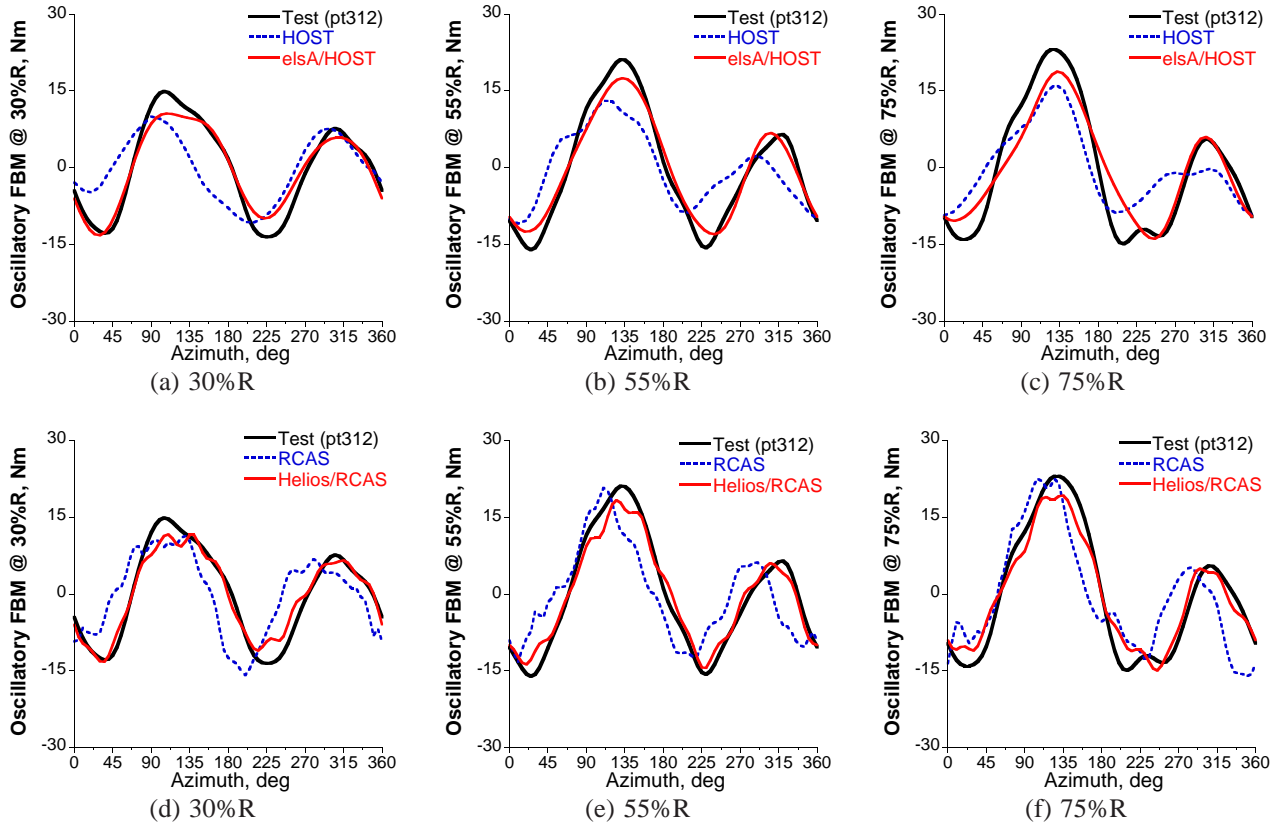


Fig. 8. Blade oscillatory flap bending moment (FBM) at high-speed condition, $\mu = 0.4$, $C_L/\sigma = 0.063$.

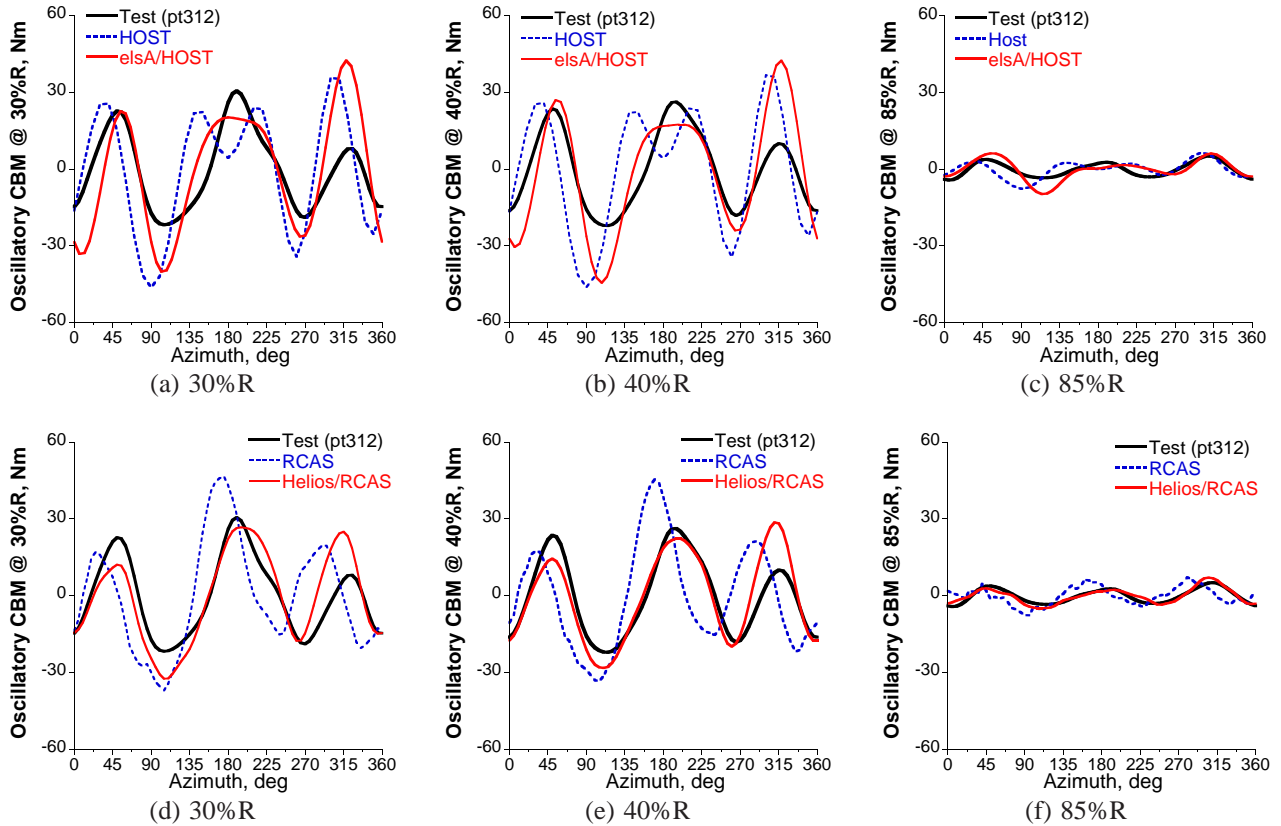


Fig. 9. Blade oscillatory chord bending moment (CBM) at high-speed condition, $\mu = 0.4$, $C_L/\sigma = 0.063$.

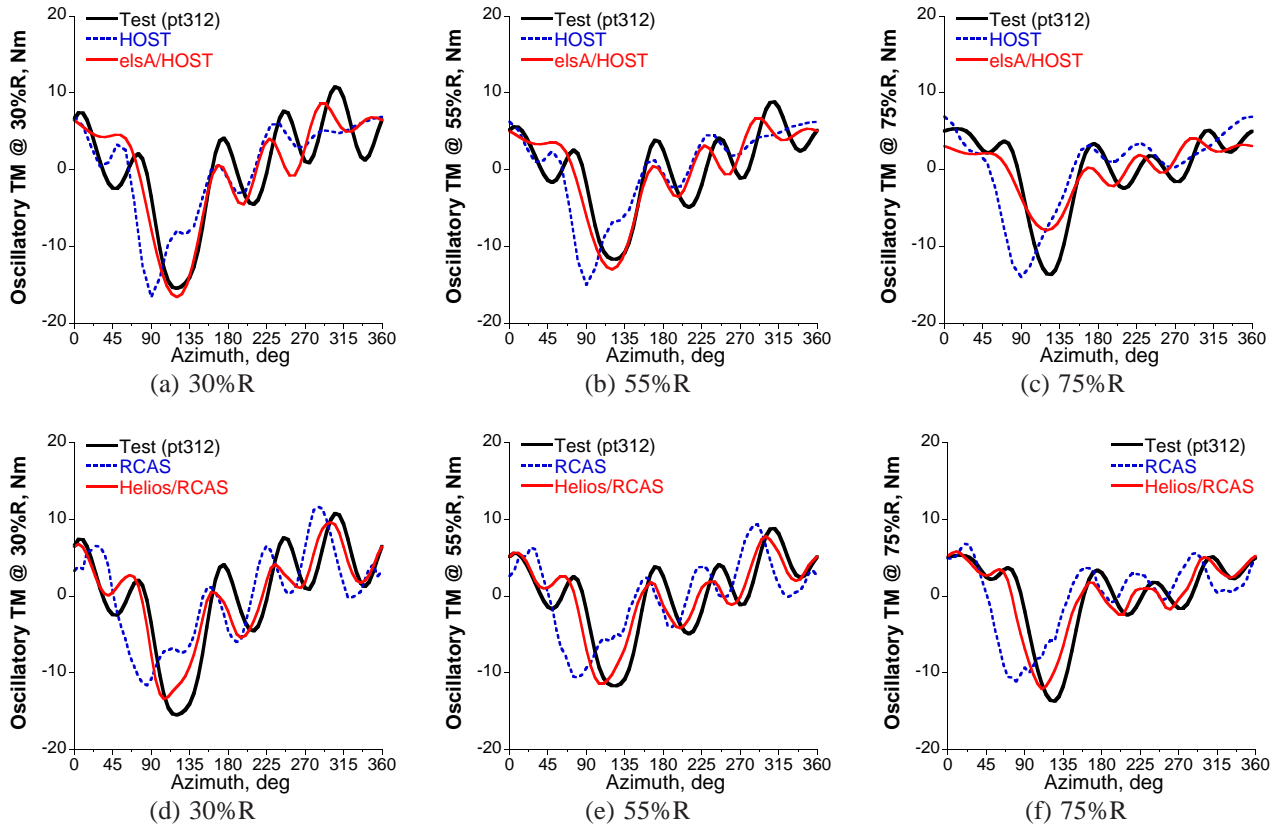


Fig. 10. Blade oscillatory torsion moment (TM) at high-speed condition, $\mu = 0.4$, $C_L/\sigma = 0.063$.

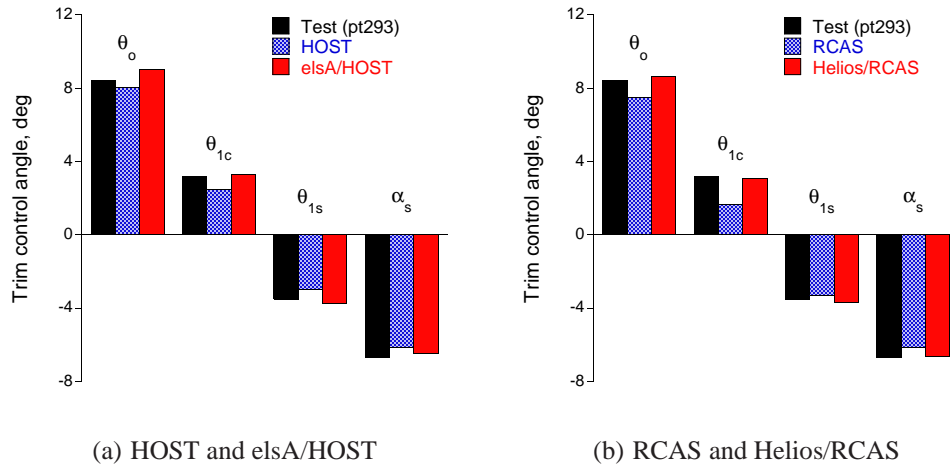


Fig. 11. Trim control angles at high-thrust condition, $\mu = 0.3$, $C_L/\sigma = 0.100$.

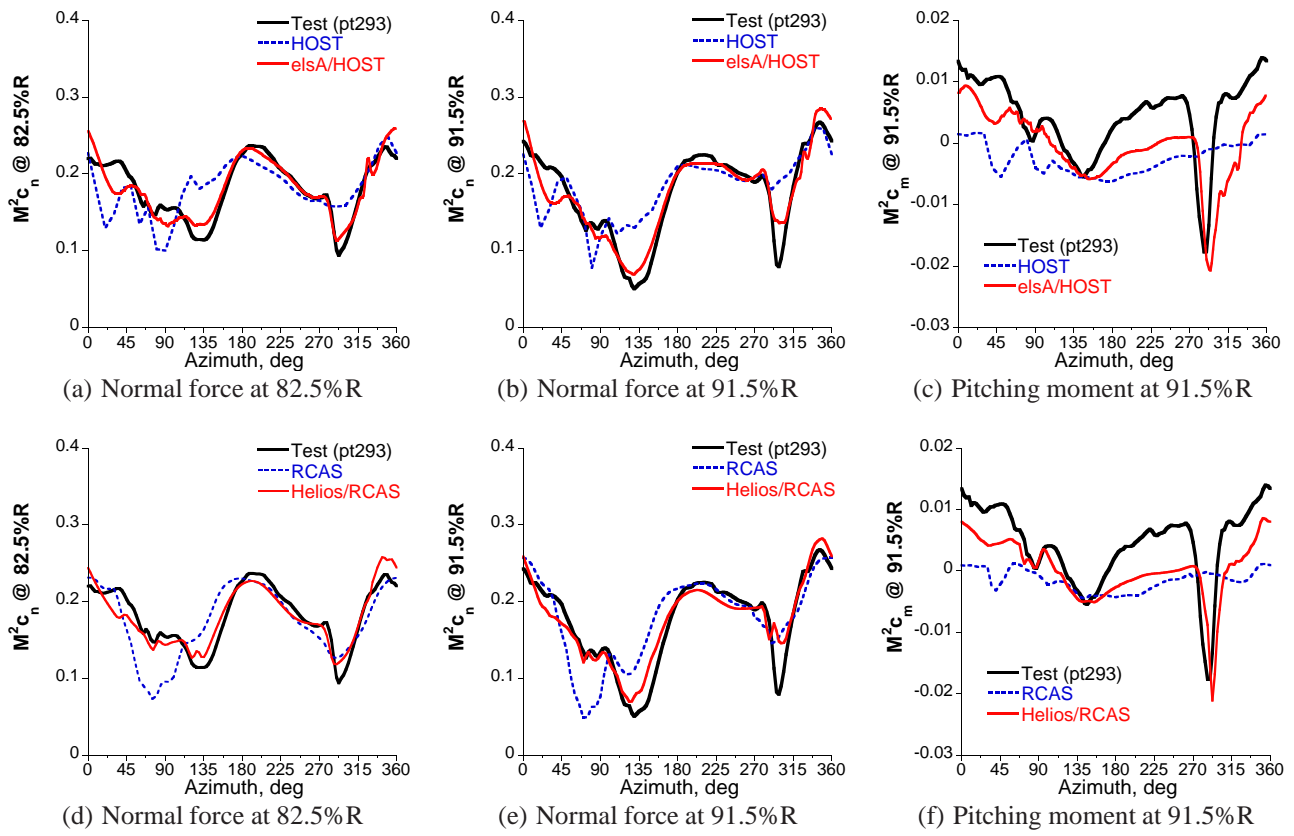


Fig. 12. Blade normal force and pitching moment at high-thrust condition, $\mu = 0.3$, $C_L/\sigma = 0.100$.

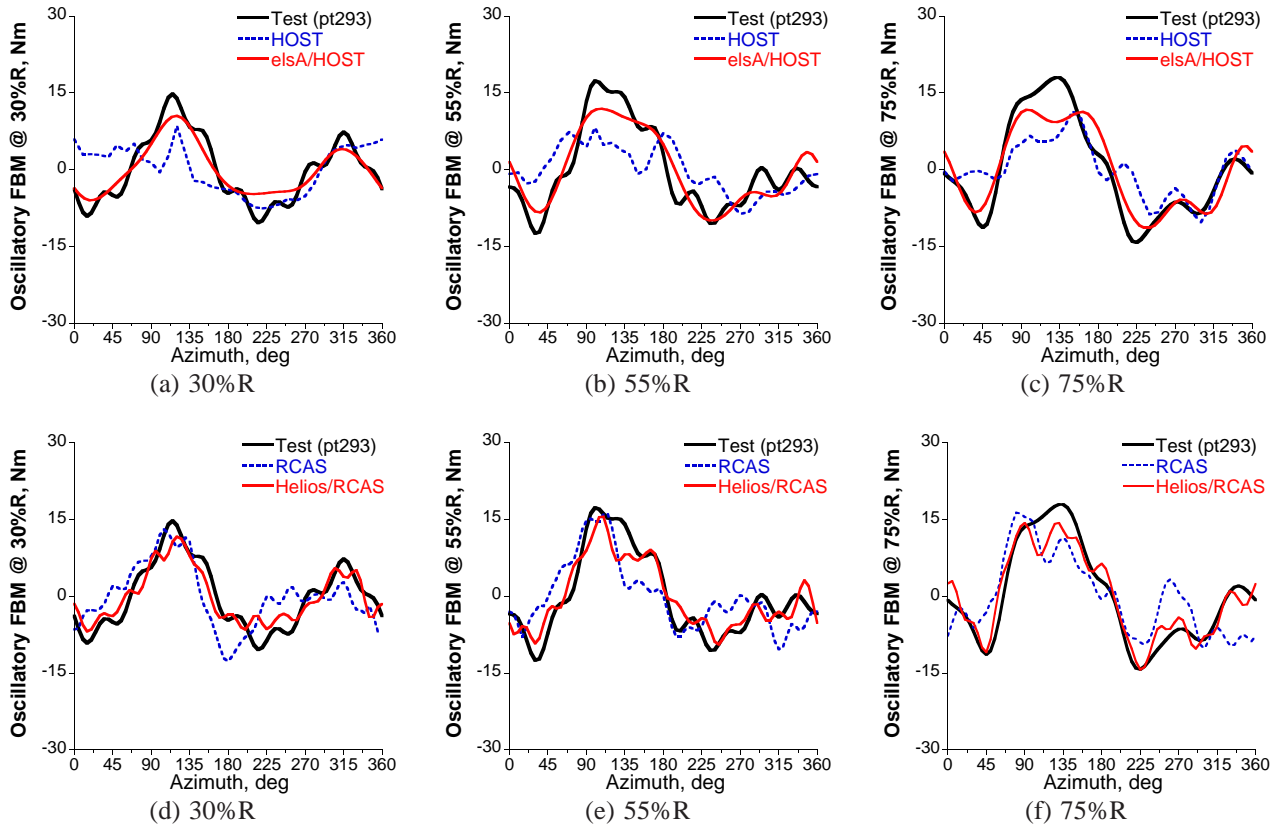


Fig. 13. Blade oscillatory flap bending moment (FBM) at high-thrust condition, $\mu = 0.3$, $C_L/\sigma = 0.100$.

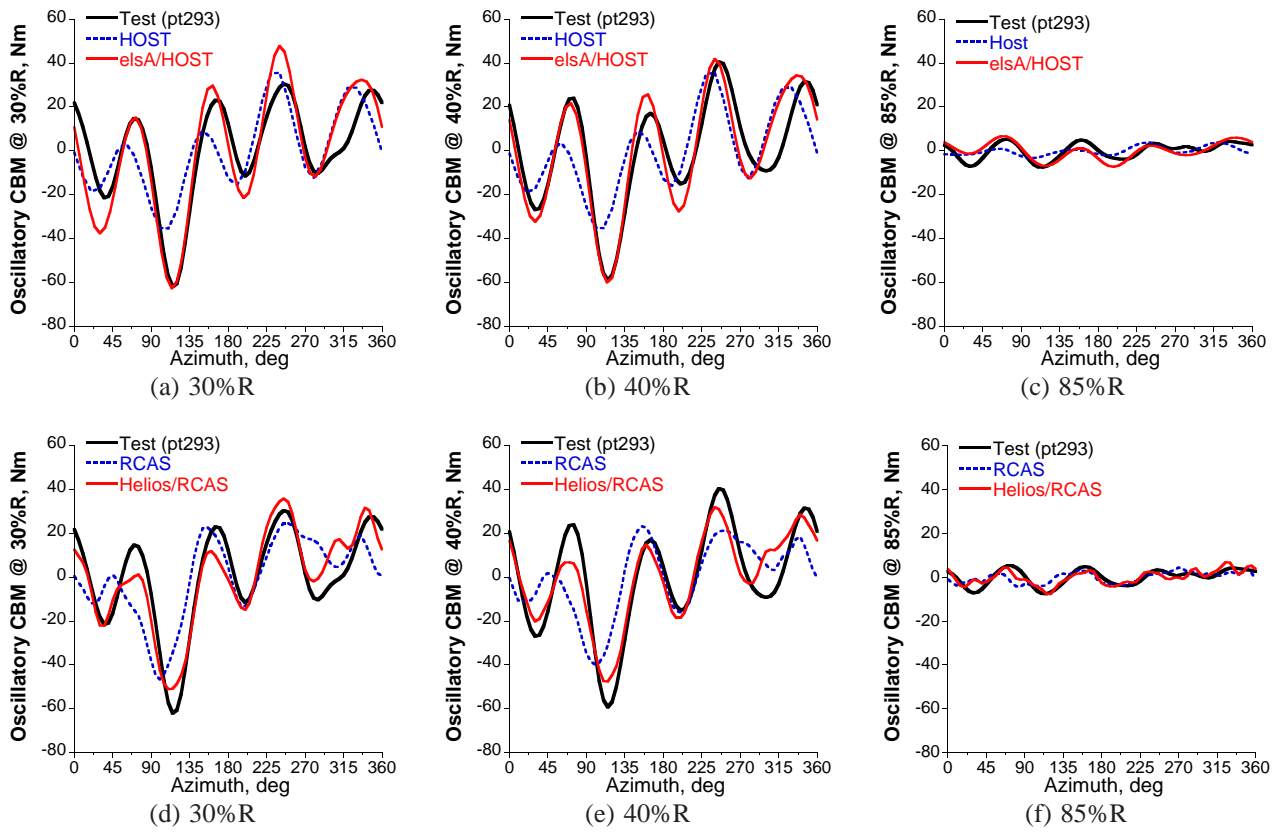


Fig. 14. Blade oscillatory chord bending moment (CBM) at high-thrust condition, $\mu = 0.3$, $C_L/\sigma = 0.100$.

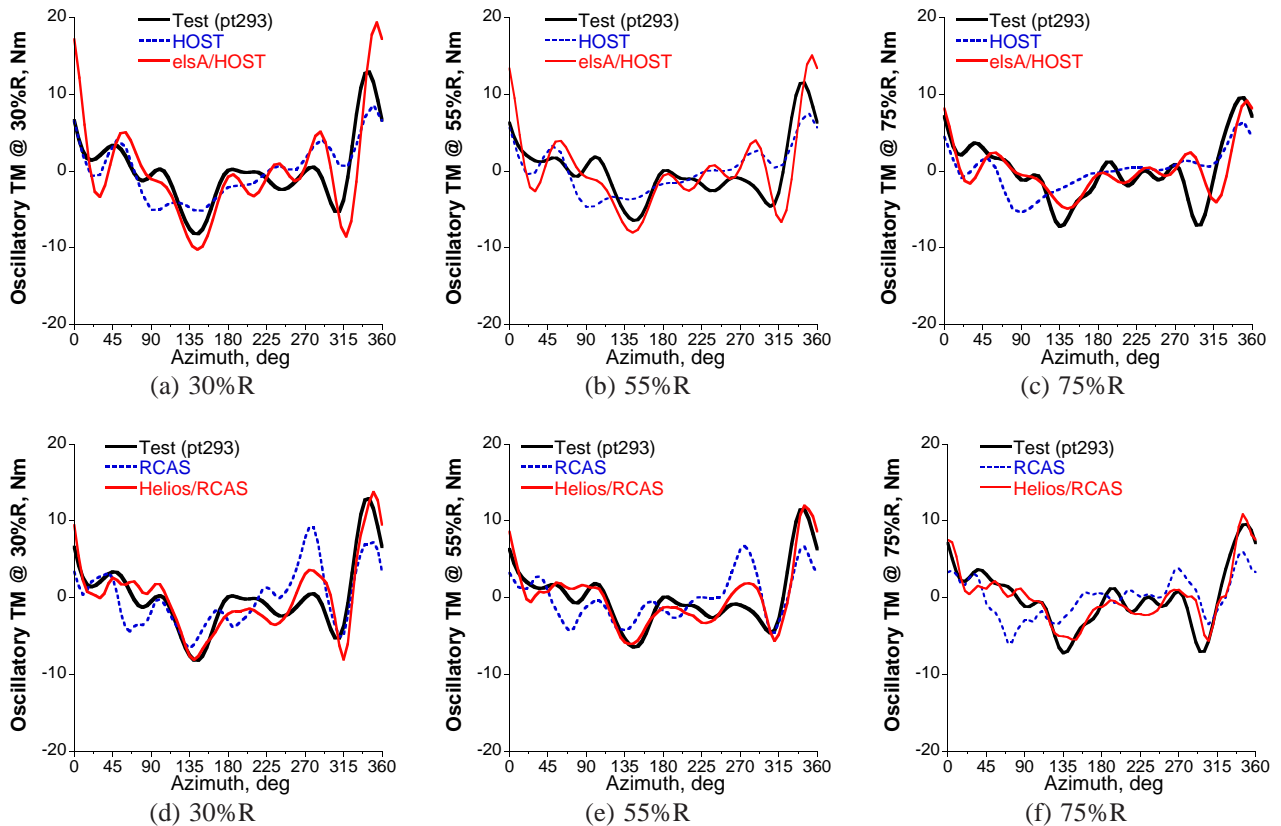


Fig. 15. Blade oscillatory torsion moment (TM) at high-thrust condition, $\mu = 0.3$, $C_L/\sigma = 0.100$.

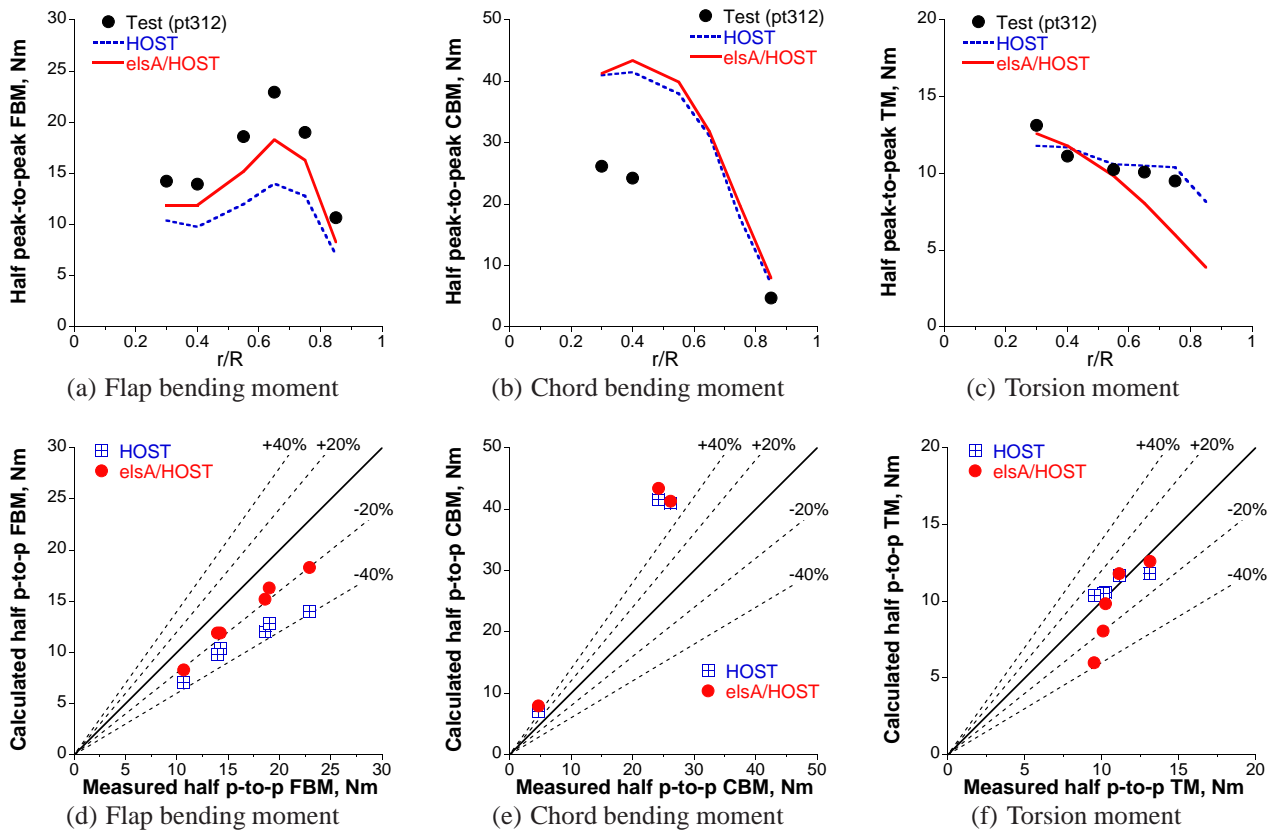


Fig. 16. Half peak-to-peak loads at high-speed condition, $\mu = 0.4$, $C_L/\sigma = 0.063$, HOST and elsA/HOST.

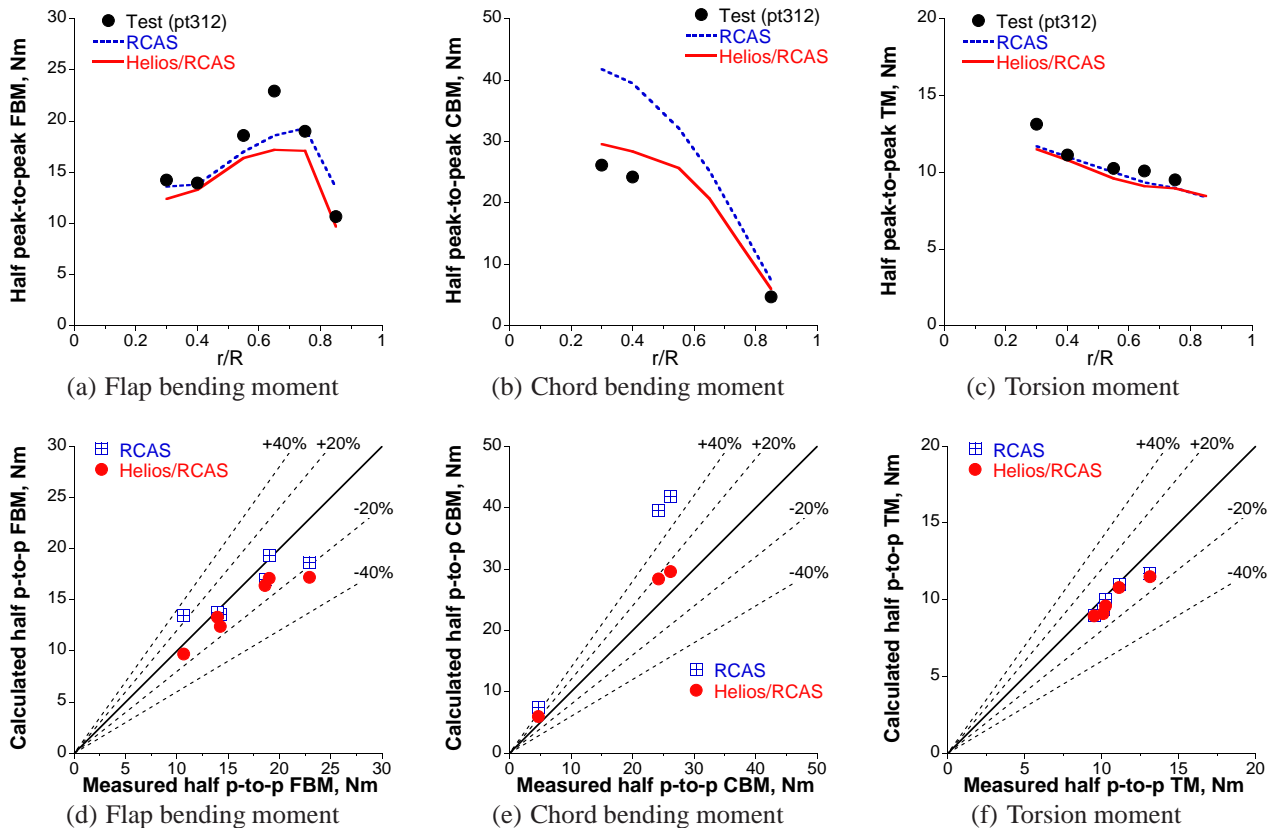


Fig. 17. Half peak-to-peak loads at high-speed condition, $\mu = 0.4$, $C_L/\sigma = 0.063$, RCAS and Helios/RCAS.

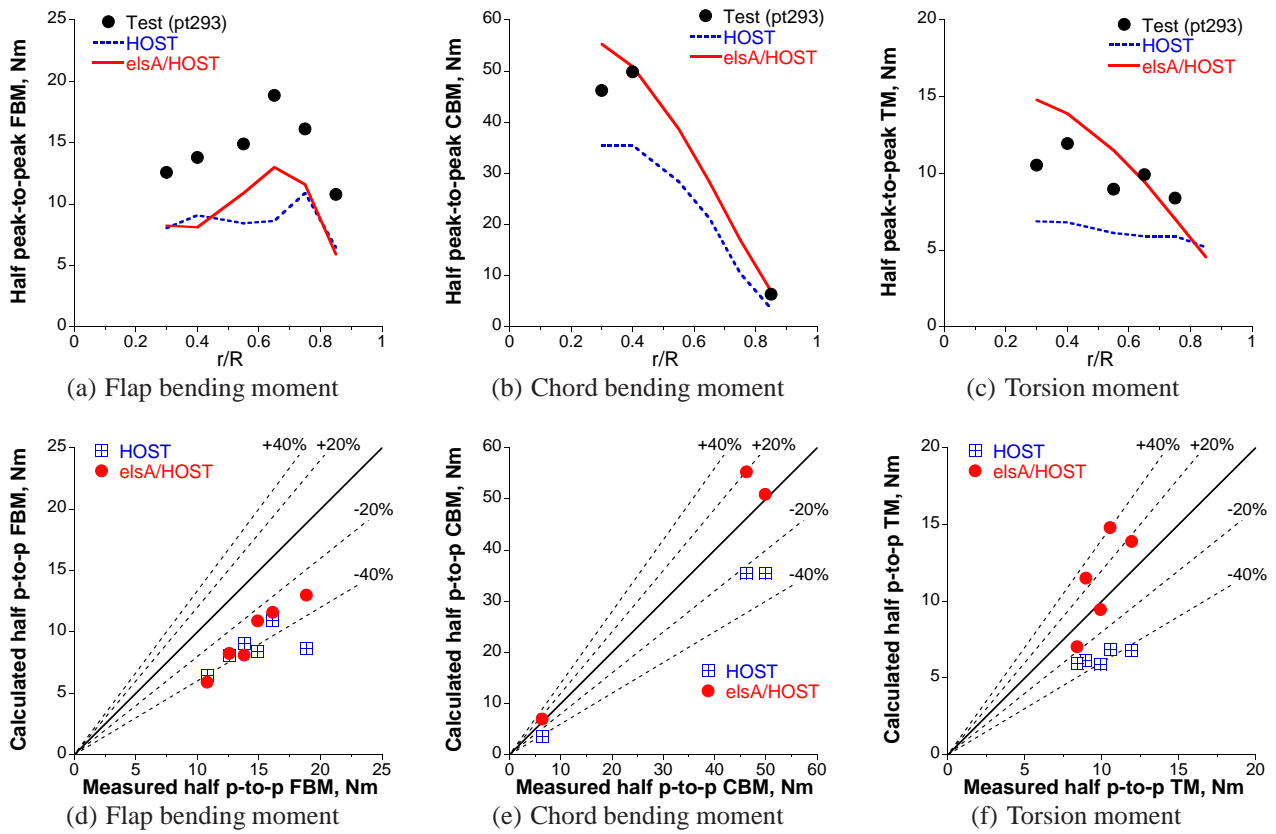


Fig. 18. Half peak-to-peak loads at high-thrust condition, $\mu = 0.3$, $C_L/\sigma = 0.100$, HOST and elsA/HOST.

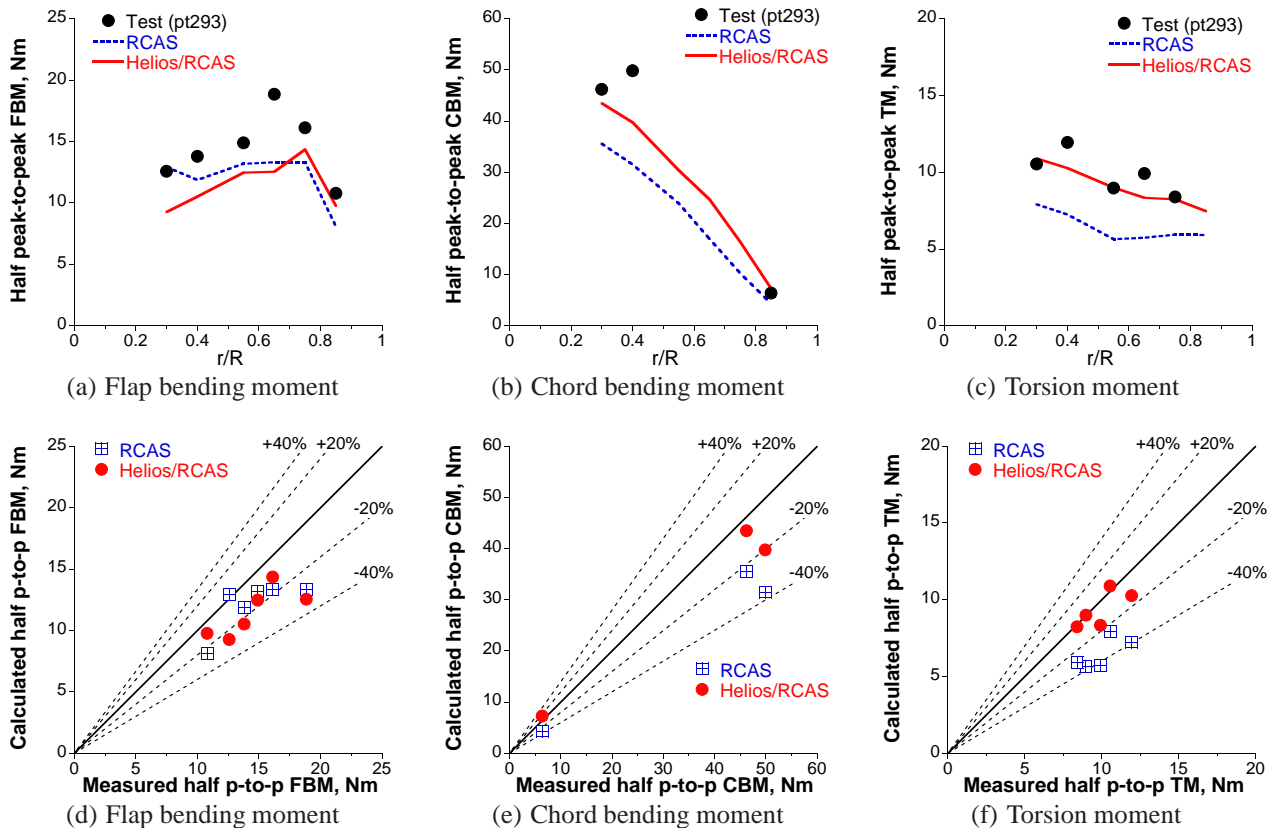


Fig. 19. Half peak-to-peak loads at high-thrust condition, $\mu = 0.3$, $C_L/\sigma = 0.100$, RCAS and Helios/RCAS.